Dynamics of alternative modes of RNA replication for positive-sense RNA viruses

Josep Sardanyés,[1,*] Fernando Martínez,[1] José-Antonio Daròs,[1] and Santiago F. Elena[1,2]

[1] *Instituto de Biología Molecular y Celular de Plantas, Consejo Superior de Investigaciones Científicas-Universitat Politècnica de València, Ingeniero Fausto Elio s/n, 46022 València, Spain*

[2] *Santa Fe Institute, 1399 Hyde Park Road, Santa Fe NM 87501, USA*

(Dated: July 15, 2011)

We propose and study nonlinear mathematical models describing the intracellular time dynamics of viral RNA accumulation for positive sense single-stranded RNA viruses. Our models consider different replication modes ranging between two extremes represented by the geometric replication (GR) and the linear stamping machine replication (SMR). We first analyze a model that quantitatively reproduced experimental data for the accumulation dynamics of both polarities of Turnip mosaic potyvirus RNAs. We identify a non-degenerate transcritical bifurcation governing the extinction of both strands depending on three key parameters: the mode of replication (α), the replication rate (r) and the degradation rate (δ) of viral strands. Our results indicate that the bifurcation associated with α generically takes place when the replication mode is closer to the SMR, thus suggesting that GR may provide viral strands with an increased robustness against degradation. This transcritical bifurcation, which is responsible for the switching from an active to an absorbing regime, suggests a smooth (i.e., second-order), absorbing-state phase transition. Finally, we also analyze a simplified model that only incorporates asymmetry in replication tied to differential replication modes.

Keywords: Complex systems; Intracellular viral dynamics; Nonlinear dynamics; Replication mode; RNA viruses; Systems biology.

I. INTRODUCTION

Multitude of theoretical and computational models considering different levels of detail and complexity layers have been proposed to better understand the dynamics of viral populations. Broadly speacking, such models can be divided in structured and unstructured. On the one hand, the structured models consider a high degree of detail in the interactions as well as in the processes governing replication and infection of viruses and have been applied to cases like the bacteriophage T7 [1, 2], human immunodeficiency virus type 1 [3], subgenomic hepatitis C virus [4], influenza A virus [5], and vesicular stomatitis virus [6]. This type of models often entail high dimensionality and a large number of parameters, which make analytical calculations and the characterization of bifurcations a difficult task. On the other hand, unstructured models can also be used to study viral dynamics in a more abstract way. As a difference from the structured ones, such models only consider the main processes tied to virus replication and/or infection, ignoring the details of the interactions, the cellular compartments where they take place or all the different macromolecules participating in the whole virus infectious cycle. Many examples of unstructured models for viruses are found in the literature (see [7–10] and references therein). This type of models, although carrying more assumptions than the structured ones, often allow for a detailed analytical characterization of the equilibrium points and their stability, thus providing clearer and valuable information about the role of the parameters in the overall dynamics of the system.

RNA viruses are obligate cellular parasites infecting bacteria, fungi, plants and animals. They are characterized by large populations, short generation times and high error rates [11–14]. The reproductive cycle of RNA viruses consists of several processes crucial for the success in replication and spreading of the virus [15]. Viruses can enter into the cell as complete particles, as ribonucleoprotein complexes or even as naked nucleic acid molecules. For the particular case of (+) sense single-stranded RNA (ssRNA) viruses such as those belonging to the picornalike group (studied in this article), the next step is the viral uncoating, by which the genome becomes available for translation, genome replication and the production of new viral particles. After infection, the genomic RNA is translated by the host ribosomes giving rise to the viral polyprotein, which is self-processed giving place to non-structural and structural proteins. The non-structural proteins give rise to the enzymes needed to replicate the genomes, a process conducted by an RNA-dependent RNA polymerase. After some rounds of amplification of the viral genomes, the structural proteins package the new genomes forming the virions, which eventually will infect other available host cells.

A key but poorly understood parameter during intracellular amplification of viral genomes is the mode of genome replication. Few studies have explored the effect of the mode of replication on the population dynamics of viral genomes from a dynamical point of view [16, 17], and even fewer experimental studies have investigated the dynamics of viral amplification quantitatively

*Corresponding author: J. Sardanyés (josep.sardanes@upf.edu).

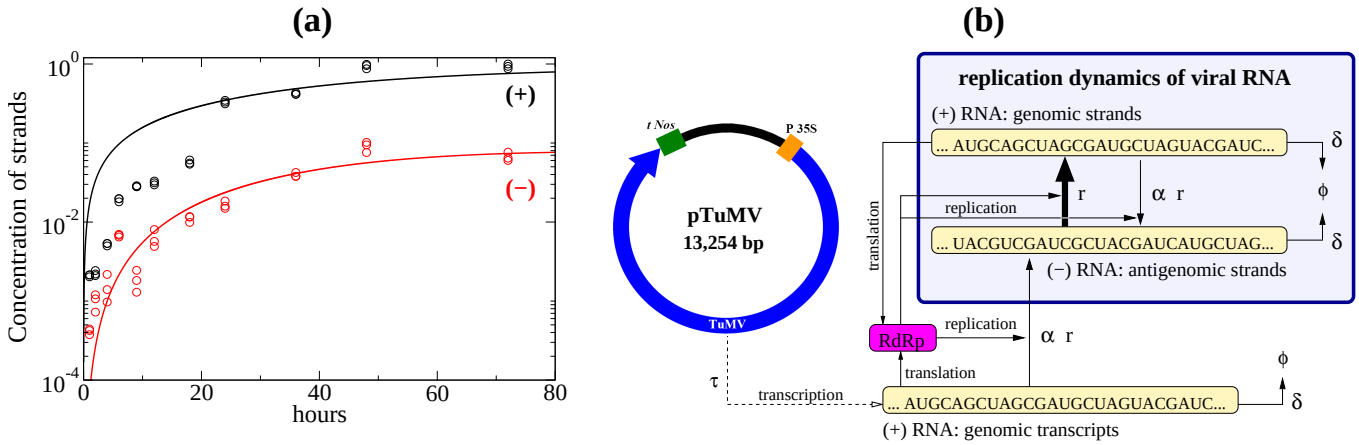

FIG. 1: (a) Intracellular dynamics of viral RNA accumulation for *Turnip mosaic virus* (TuMV). Black and red circles correspond, respectively, to normalized experimental data for (+) and (-) sense strands (see [18]). Black and red lines show the fitting obtained numerically from Eqs. (1)-(2) using $\alpha = 0.0642$ (see [18] for the other parameter values). (b) Schematic diagram of the system under study. In the experiments, a plasmid was used to produce a viral transcript responsible for initiating the process of viral replication, which starts once the RNA-dependent RNA-polymerase (RdRp) is translated from the RNA transcript. The blue box displays a schematic diagram of the processes analyzed in this study using Eqs. (3)-(4). Our model considers strands' replication at a rate $r > 0$. To include the replication mode we use parameter $\alpha \in (0, 1]$. When $\alpha = 1$ the replication is geometric because it is equal for both types of strands. If $\alpha \to 0$, the production of strands is mainly from (-) to (+) strands, in the stamping machine mode. We also include degradation of the strands proportional to the parameter $\delta > 0$.

[18]. Nevertheless, the few available data suggest different models of replication for different viruses such as the stamping machine replication (hereafter SMR) mode. For SMR, and considering an infecting virus with a (+) sense RNA genome, the progeny of strands will be synthesized from (-) strand complementary to the infecting (+) sense genome, and thus the expected fraction of mutant genomes produced per infected cell follows $1 - e^{-\mu}$, being μ the genomic mutation rate. In this case, the distribution of mutants per infected cell before the action of selection follows a Poisson distribution. Such a distribution was identified for bacteriophage ϕX174 [20]. Another suggested mode of replication, opposed to the SMR, is the geometric replication (hereafter GR) mode. For GR, both (+) and (-) sense RNA strands are used as templates for viral amplification. For this mode of replication, the expected fraction of mutants genomes produced per infected cell depends on the number of replication cycles, n, according to expression $1 - e^{-n\mu}$. The resulting distribution of mutants then follows the Luria-Delbrück distribution. Deviations from the Poisson distribution were found for the phage $T2$ [21], thus suggesting that such a virus replicates according to the GR model. Intermediate modes of replication may also exist, as described for bacteriophage $\Phi 6$ [22]. In this case, the distribution of mutants slightly deviated from the Poisson distribution, thus suggesting that the replication was mainly achieved by an SMR strategy plus a small contribution of GR.

A direct experimental evaluation of the mode of replication for an eukaryotic RNA virus has only been provided very recently. Martínez et al. [18] monitored and quantified the accumulation of both RNA polarities of *Turnip mosaic virus* (TuMV) infecting protoplasts of the plant *Nicotiana benthamiana*. There, we developed a simple dynamical system describing the production of (-) and (+) sense RNA strands including constitutive transcription of (+) strands from a plasmid and interference of (+) strands on the synthesis of (-) ones (see Section II). Such model was used to fit the experimental data [Fig. 1(a)]. In the present study we first analyze a simplified version of this model that may be useful to better understand the within-cell dynamics (+) sense RNA viruses. We analyze in detail the dynamics of the model, studying the equilibrium points and their stability depending on key parameters governing the intracellular dynamics of viral RNA replication, paying especial attention to the role of the replication mode. In short, we characterize a non-degenerate transcritical bifurcation governing the shift from an active phase, where both viral strands coexist, to an absorbing state, for which both sequences become extinct. The critical expression responsible for the bifurcation depends on the assymetry of replication (i.e., the replication mode), on the replication rate as well as on RNA degradation rates. Our results suggest that SMR is more sensitive to the bifurcation and thus GR confers viral genomes with a dynamical advantage. We finally analyze a simpler model that only considers the mode of replication, also studying its equilibria and stability properties.

II. MATHEMATICAL MODEL

In this section we will introduce a mathematical model that we recently used to fit experimental data on the accumulation for TuMV genomic (+) and antigenomic (-) RNAs [18]. The model describes the time dynamics of well-mixed populations of (+) and (-) strands during intracellular viral amplification considering key parameters such as different replication modes and degradation of viral strands in the limit of infinite diffusion [see Fig. 1(b)]. The model is given by the next couple of nonlinear differential equations:

$$\frac{dp}{dt} = (\tau + rm)\Phi(p,m) - \delta_p p, \tag{1}$$

$$\frac{dm}{dt} = \frac{\alpha r}{1+\psi p} p\Phi(p,m) - \delta_m m. \tag{2}$$

The state variables p and m denote, respectively, the concentration of (+) (p: plus) and (-) (m: minus) strands. Note that for simplicity we obviate the intermediates of replication given by double stranded RNAs as well as the explicit consideration of mutation. We consider that the replication of the viral RNA is constrained by a logistic-like function, given by:

$$\Phi(p,m) = 1 - (p+m)/K,$$

assuming finite resources. Here, K is the cellular carrying capacity. The parameter $r > 0$ corresponds to the replication rate of the strands, which is assumed to be symmetric. However, we introduce the parameter α (with $0 < \alpha \leq 1$) in Eq. (2) to model all the scenarios of asymmetric replication between the GR mode (with $\alpha = 1$ i.e., both strands replicate at the same rate) and the SMR mode (with $\alpha \gtrapprox 0$). For this latter case, the replication proceeds mainly from (-) to (+) strands. Finally, the model also considers, respectively, that (+) and (-) sense strands are degraded at rates $\delta_p > 0$ and $\delta_m > 0$.

Equations (1)-(2) provide a simple scheme to study the dynamics of the strands during intracellular viral replication considering asymmetries in the replication rates due to different replication modes. As we mentioned in the Introduction, this model was successfully applied to reproduce experimental data obtained during the amplification phase of TuMV in *N. benthamiana* protoplasts [18] [see Fig. 1(a)]. In that work we estimated key parameters in the replication of this virus, especially the mode of replication. The parameter τ was introduced because in the experiments viral infection was initiated by the constitutive transcription of (+) strands from an infectious cDNA containing the viral genome (Fig. 1). Moreover, the term $1/(1+\psi p)$ was introduced in Eq. (2) to account for possible interference of (+) strands in the synthesis of (-) strands that could result in differences between the two RNA accumulation curves. The inference of parameter ψ (which measures the negative effect of accumulating (+) strands on the synthesis of the (-) ones) indicated that no major interference existed, and thus that the differences in accumulation observed between the two strands emerged mainly from the different replication modes [18].

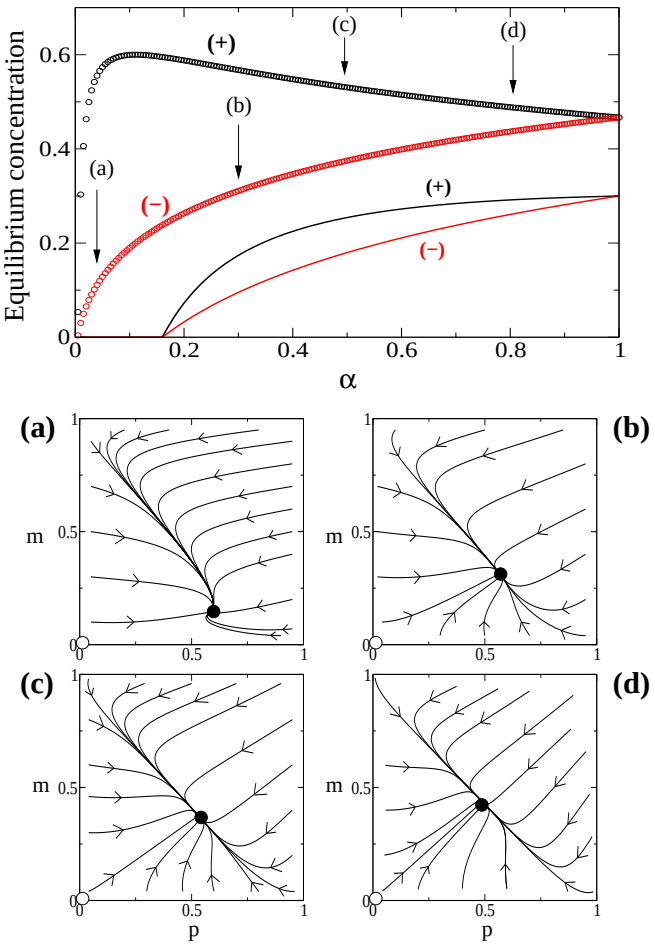

FIG. 2: (Top panel) Bifurcation diagram for Eqs. (3)-(4) showing the equilibrium concentration for (+) (p, black) and (-) (m, red) strands using α as control parameter with $\delta = 0.05$ and: $r = 0.75$ (circles); $r = 0.1249$ (thin lines) (for all data points we use $p(0) = 0.1$ and $m(0) = 0$ as initial conditions). Below we show four phase portraits in $\mathbf{\Gamma}$ for several values of α indicated with the arrows in the bifurcation diagram: (a) $\alpha = 0.06$, (b) $\alpha = 0.3$, (c) $\alpha = 0.5$, (d) $\alpha = 0.8$ (using $r = 0.75$ and $\delta = 0.05$). In all the phase portraits the origin is unstable and the fixed point P_+^* is a stable node. The arrows indicate the direction of the flows.

Given that interference was not significant in the TuMV system, in the following, we will not consider it (i.e., $\psi = 0$). Moreover, the strand initiating the process of viral replication for (+) sense ssRNA viruses in natural infections is the (+) genome of the virus. Henceforth, in our analyses we will set $\tau = 0$, and the biologically meaningful initial conditions will be $p(0) > 0$ and $m(0) = 0$.

III. RESULTS

A. Analyses with degradation of strands

In this section we provide analytical and numerical results to characterize the dynamics of Eqs. (1)-(2) (with $\psi = 0$, $\tau = 0$ and $\delta_m = \delta_p \equiv \delta$). We note that setting $\delta_p = \delta_m \equiv \delta$, allows for a clearer identification of the effect of the mode of replication on the population dynamics of the two strands, which is the central question we sought to address in this study. Hence, the dynamical system we will explore is given by:

$$\frac{dp}{dt} = rm\left(1 - \frac{p+m}{K}\right) - \delta p, \tag{3}$$

$$\frac{dm}{dt} = \alpha rp\left(1 - \frac{p+m}{K}\right) - \delta m. \tag{4}$$

The concentration variables or population numbers span the two-dimensional open space:

$$\mathbb{R}^2 : \{p, m; -\infty < p, m < \infty\},$$

only part of which is physically meaningful:

$$\mathbf{\Gamma} \in \mathbb{R}^2; \mathbf{\Gamma} := \{p, m \in \mathbb{R}^+ : 0 \leq p, m \leq 1\}.$$

According to the logistic-like constraint (hereafter assuming $K = 1$), the biologically meaningful equilibrium points live into the triangular phase plane, $\mathbf{\Gamma}_K \in \mathbf{\Gamma}$, with:

$$\mathbf{\Gamma}_K := \{p, m \in \mathbb{R}^+ : 0 \leq p + m \leq K = 1\}.$$

It can be shown that the system of Eqs. (3)-(4) has three fixed points or equilibria, which are calculated from $dp/dt = 0$ and $dm/dt = 0$. The first equilibrium is the trivial one, given by $P_1^* = (0, 0)$, which involves, if stable, the extinction of both types of strands. The other two fixed points, denoted as $P_\pm^* = (p_\pm^*, m_\pm^*)$, are given by:

$$p_\pm^* = \frac{-r\alpha(r+\delta) \pm \gamma}{\beta\alpha},$$

with:

$$\gamma = r(r\alpha + \delta)\sqrt{\alpha} \quad \text{and} \quad \beta = r^2(\alpha - 1),$$

and:

$$m_\pm^* = \pm\frac{r\sqrt{\alpha} \mp \delta}{r \pm r\sqrt{\alpha}}.$$

The next step is to study the stability of these equilibrium points, which will depend on the model parameters. To do so, we perform linear stability analysis, evaluating the Jacobian matrix at each of the equilibrium points of the system. The general form of the Jacobian matrix for the dynamical system under study is given by:

$$J = \begin{pmatrix} -rm - \delta & r(1 - p - 2m) \\ \alpha r(1 - 2p - m) & -\alpha rp - \delta \end{pmatrix}.$$

The equilibria can be categorized as stable or unstable depending on the sign of the resulting eigenvalues. For a two-dimensional dynamical systems like the one in hands, two negative eigenvalues mean that the fixed point is stable. However, if one or both eigenvalues are positive, then such an equilibrium will be unstable, and initial conditions in the close vicinity of this fixed point will move away from this equilibrium. The general expressions of the eigenvalues, obtained from $\det(J - \lambda I) = 0$, take the form:

$$\lambda_\pm = \frac{1}{2}\left(r(-m - p\alpha \pm \sqrt{\omega}) - 2\delta\right),$$

with

$$\omega = m^2 + \alpha[4 + p(p\alpha + 8p + 18m - 12) - 4m(3 - 2m)].$$

The corresponding eigenvectors are:

$$\nu_\pm = \left\{-\frac{-m + p\alpha \pm \sqrt{\omega}}{2\alpha(m + 2p - 1)}, 1\right\}.$$

We can study the qualitative behavior of Eqs. (3)-(4), especially for those scenarios of extinction and persistence of both strands. To do so, and for simplicity, we first study the stability of the trivial fixed point, $P_1^*(0, 0)$, with linear stability analysis, while the stability of the other equilibria is numerically studied (all numerical results shown in this study are obtained using the fourth-order Runge-Kutta method with a time stepsize $\Delta t = 10^{-2}$).

It can be shown that the two eigenvalues evaluated at the trivial equilibrium point (i.e., computed from $\det(J(\mathbf{0}) - \lambda I) = 0$) are $\lambda_\pm = -\delta \pm r\sqrt{\alpha}$, and the eigenvectors are $\nu_\pm = \{\pm(\sqrt{\alpha})^{-1}, 1\}$. Note that λ_- is always negative because of the positivity of all parameters. Hence, the stability of the equilibrium point P_1^* entirely depends on λ_+. From this second eigenvalue we can compute the critical value of the mode of replication, α_c, associated to the changes in the stability of the extinction equilibrium given by P_1^*. Such a critical value is given by:

$$\alpha_c = (\delta/r)^2. \tag{5}$$

From the previous calculations it follows that if $\alpha < \alpha_c$ then $\lambda_+ < 0$, and the origin will be stable because $\lambda_\pm < 0$, and both strands will become extinct. However, if $\alpha > \alpha_c$ then $\lambda_+ > 0$, the origin will be a saddle and the flows will be attracted by the equilibrium point P_+^*, which is a stable node (Fig. 2). Figure 2 shows that when the replication mode gets closer to the SMR ($\alpha \to 0$), the asymptotic concentration of (+) sense strands increases much more pronouncedly than the concentration of (-) sense strands. Moreover, when the system is analyzed

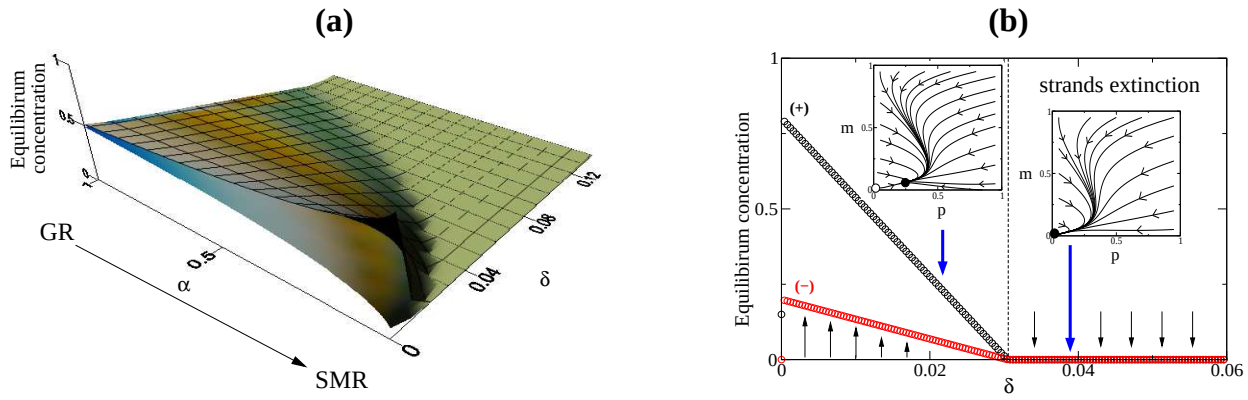

FIG. 3: (a) Equilibrium concentration of (+) sense (gridded surface) and (-) sense (flat surface) strands using α (with $0 < \alpha \leq 1$) and δ as control parameters with $r = 0.1249$. Initial conditions: $p(0) = 0.15$ and $m(0) = 0$. (b) Bifurcation diagram numerically obtained form Eqs. (3)-(4), using the equilibrium concentration of both strands as order parameters ($y - axis$) and δ as control parameter ($x - axis$). We use the values $r = 0.1249$ and $\alpha = 0.0642$ (as in the previous figure). The small arrows indicate the stability of the trivial equilibrium point. The vertical dashed line shows the critical degradation value, δ_c, given by Eq. (7) (under the selected parameter values, $\delta_c \approx 0.03164\cdots$). The insets show the phase portraits for two different values of degradation rate (indicated with the blue arrows). For the case $\delta < \delta_c$, we use: $\delta = 0.022$; for the extinction scenario we use: $\delta = 0.037 > \delta_c$. Henceforth, stable and unstable equilibria in the phase portraits will be displayed, respectively, with black and white solid circles.

for values of α closer to 1 (i.e., closer to a purely geometric replication), the equilibria of both strands get closer. The bifurcation diagram of Fig. 2 indicates that the decrease of α below the critical value given by Eq. (5) results in the extinction of the two strands (see thin lines in the bifurcation diagram of Fig. 2). The presence of a critical value of the mode of replication responsible for the switch between coexistence to extinction allows to interpret such a change as a standard *absorbing-state phase transition*. This is a class of nonequilibrium transition in which the system crosses from an active to an absorbing phase, by the variation of a control parameter. Once the absorbing phase is achieved, the system remains in such a phase forever, with no possibility to escape [19] (see the description of the bifurcation below). For the selected parameters ($r = 0.1249$ and $\delta = 0.05$), $\alpha_c = 0.1602\cdots$. If the parameter $\alpha < \alpha_c$, the populations of strands can not self-maintain and becomes extinct. That is, a decrease of α entailing the approach to the SMR mode causes the extinction of the whole populations of viral strands.

Similarly as we did for the parameter tied to the mode of replication, we can also obtain the critical values of replication rate as well as of degradation rate responsible for the extinction of the strands. The critical values for these two parameters are given, respectively, by:

$$r_c = \delta\alpha^{-1/2}, \tag{6}$$

and

$$\delta_c = r\sqrt{\alpha}. \tag{7}$$

If $r > r_c$: $\lambda_+ > 0$, and the trivial equilibrium point will be a saddle point (recall that $\lambda_- < 0$). If $r < r_c$: $\lambda_+ < 0$, and then the origin will be stable because both eigenvalues are negative. For the degradation parameter, the trivial fixed point will be stable if $\delta > \delta_c$. However, if $\delta < \delta_c$, $\lambda_+ > 0$ and then the trivial equilibrium will be a saddle. Under this scenario, the two RNA strands will achieve a non-trivial steady state. Such steady state is given by the fixed point P_+^*. Actually, the third fixed point, P_-^*, is outside the phase plane $\mathbf{\Gamma}$: the second coordinate of the equilibrium point P_-^*, which corresponds to the equilibrium concentration of the (-) sense strands, is always negative under the biologically meaningful ranges of the parameters. Note that under the ranges $0 < \alpha < 1$, $r\sqrt{\alpha} < r$, and the denominator of the coordinate m_-^* will be always positive. Hence m_-^* will be always negative.

The dynamics of Eqs. (3)-(4) are illustrated in Figs. 2 and 3 by means of the solutions obtained numerically. Some illustrative examples of the dynamics arising using differential values of α, parameterizing differential replication modes, are shown in Fig. 2. As previously mentioned, the equilibrium concentration between both (+) and (-) strands largely differs when α is near 0, and thus replication proceeds via SMR. As α grows towards one, the concentration of both strands become more similar, being equal for $\alpha = 1$, which actually correspond to the pure GR. In the analyses shown in Fig. 2 the degradation rate of the strands is below the critical value, and the equilibrium points of $\mathbf{\Gamma}_K$ are an unstable fixed point (the origin) and the stable node P_+^*. The phase portraits shown in Figs. 2(a)-(d) display the effect of increasing α: the stable node travels towards symmetric equilibrium values for both strands. We note that the dynamics associated to the meaningful equilibria for Eqs. (3)-(4) (given by the origin and P_+^*) are independent of the initial conditions. It means that from any arbitrary initial

condition, the flows will achieve a single attractor depending on whether the system is in the survival or in the extinction scenario.

Figure 3(a) shows the equilibrium concentration of both types of strands in the parameter space (α, δ). In agreement with the results reported above, two different scenarios are found: (i) survival and (ii) extinction of strands. Scenario (i) occurs for those values of $\delta < \delta_c$, and the dynamics asymptotes towards the non-trivial steady state given by P_+^*. As we discussed above, for a given value of δ and r, the system will become extinct as α is decreased and the replication gets closer to the SMR mode. An interesting result shown in Fig. 3(a) is that GR confers a higher resistance to degradation. This is due to the fact that all produced strands are used as templates for further replication. On the contrary, for the SMR mode, only a small fraction of (-) sense strands are used as templates and thus the population is much more sensitive to degradation.

The results from linear stability analysis and from the bifurcation diagram shown in Figs. 2 and 3(b) suggest that the transition from survival to extinction of strands associated to the critical parameters previously characterized is governed by a transcritical bifurcation. The transcritical bifurcation occurs when two equilibrium points collide and interchange their stability [23]. This type of bifurcation suggests the presence of a smooth, absorbing-state phase transition because the order parameter (i.e., equilibrium values of both types of strands) decrease in a continuous way as the control parameter is driven towards its bifurcation value, and no sharp transitions occur as one might found for saddle-node bifurcations tied to first-order phase transitions. For our system, it can be shown that

$$P_+^*|_{\alpha_c=(\delta/r)^2} = (p_+^* = 0, m_+^* = 0). \tag{8}$$

Hence, at the critical value of the parameter tied to the replication mode, both fixed points P_1^* and P_+^* collide. The stability of the fixed point P_+^* was numerically investigated by evaluating the sign of the two eigenvalues from

$$\lambda_\pm(P_+^*) = \frac{1}{2}\left[r\Big(-m_+^* - p_+^*\alpha \pm \sqrt{\omega|_{(p_+^*, m_+^*)}}\Big) - 2\delta\right],$$

with:

$$\omega|_{(p_+^*, m_+^*)} = m_+^{*^2} + \alpha[4 + p_+^*(p_+^*\alpha + 8p_+^* + 18m_+^* - 12) - 4m_+^*(3 - 2m_+^*)].$$

Numerical computations of the eigenvalues for the fixed point P_+^* using the same parameter range shown in the bifurcation diagram of Fig. 2 were performed, obtaining (results not shown):

$$\lambda_-(P_+^*) < 0; \lambda_+(P_+^*)|_{\alpha<\alpha_c} > 0; \lambda_+(P_+^*)|_{\alpha=\alpha_c} = 0,$$

and: $\lambda_+(P_+^*)|_{\alpha>\alpha_c} < 0$. Moreover, the study of the eigenvalues in the parameter range studied in Fig. 3(b) (i.e., $0 \leq \delta \leq 0.06$), also indicated that $\lambda_-(P_+^*)$ was always negative, and that

$$\lambda_+(P_+^*)|_{\delta<\delta_c} < 0; \lambda_+(P_+^*)|_{\delta=\delta_c} = 0; \lambda_+(P_+^*)|_{\delta>\delta_c} > 0,$$

(results not shown). The two insets of Fig. 3(b) show, respectively, the phase portraits for the scenarios of survival and extinction of the strands (we show the flows in the phase plane $\mathbf{\Gamma}$). The origin with $\delta < \delta_c$ is an unstable equilibrium (indicated with a white circle), and the non-trivial equilibrium P_+^* is a stable node (indicated with a black circle). Once the degradation rate overcomes the critical value, the equilibrium P_+^* goes outside the phase plane $\mathbf{\Gamma}$, and P_1^* becomes stable.

All the previous analyses indicate that the fixed points P_1^* and P_+^* collide at the critical parameter values and that one eigenvalue (i.e., λ_+) interchanges its stability. Under such conditions the transcritical bifurcation is called non-degenerate. The same type of transition occurs as the other two parameters (i.e., r and δ) cross their critical values given by Eqs. (6) and (7). From Eq. (8), we also obtain:

$$P_+^*|_{r=r_c} = (0,0) \quad \text{and} \quad \mathrm{P}_+^*|_{\delta=\delta_c} = (0,0).$$

B. Analyses without degradation of strands

Since we are manly interested in the dependence between the viral RNA dynamics and the asymmetry in the mode of replication, we further simplify the model by only keeping parameter α, and assuming r=1 and $\delta = 0$. The parameters estimated in [18] revealed that the degradation rates of the viral RNAs were approximately between one and two orders of magnitude lower than the replication rate. Hence, the assumption $\delta = 0$ is a first good approach to study the simplest model of viral strands amplification under differential replication modes. The model is then simplified to the following couple of dynamic equations (also setting K=1):

$$\frac{dp}{dt} = m(1 - p - m), \tag{9}$$

$$\frac{dm}{dt} = \alpha p(1 - p - m). \tag{10}$$

The dynamical system above has four fixed points given by:

$$P_a^* = (0,0), \;\; P_b^* = (0,1), \;\; P_c^* = (1,0),$$

and

$$\mathbf{P}_d^* = (1 - m^*, m^*).$$

Note that all the points of the form $(1 - m^*, m^*)$, that is, $p^* = 1 - m^*$ (which is the diagonal border in $\mathbf{\Gamma}_K$), are

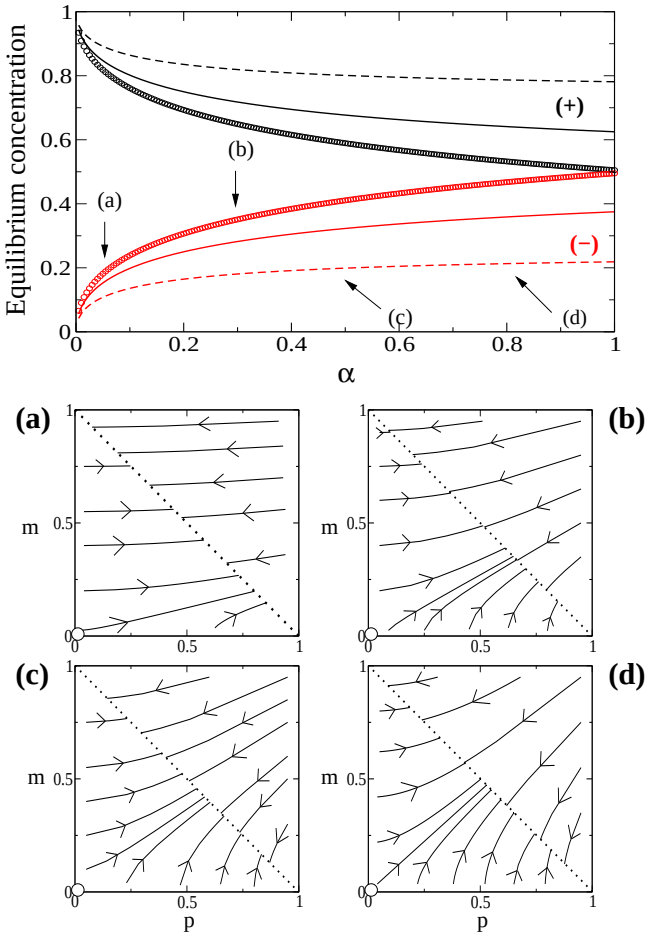

FIG. 4: Same as in Fig. 3 for the simplified model given by Eqs. (9)-(10). The upper panel shows the two equilibria for (+) (black) and (-) (red) strands using three different initial conditions for the (+) sense strands (all of them with $m(0) = 0$): $p(0) = 0.1$ (circles), $p(0) = 0.5$ (solid lines) and $p(0) = 0.7$ (dashed lines). Phase portraits for the same values of α analyzed in Fig. 3, also indicated with arrows in the bifurcation diagram: (a) $\alpha = 0.06$, (b) $\alpha = 0.3$, (c) $\alpha = 0.5$ and (d) $\alpha = 0.8$. The diagonal displayed with the thick dotted line corresponds to the line of equilibria, $\mathbf{P}_d^* = (1 - m^*, m^*)$.

equilibrium points. The Jacobian matrix for this reduced model is given by:

$$J = \begin{pmatrix} -m & 1-p-2m \\ \alpha(1-2p-m) & -\alpha p \end{pmatrix}. \qquad (11)$$

The eigenvalues of matrix (11) have the general form

$$\lambda_\pm = \frac{1}{2}\left(-m - p\alpha \pm \sqrt{\omega}\right),$$

(here also with $\omega = m^2 + \alpha[4 + p(p\alpha + 8p + 18m - 12) - 4m(3 - 2m)]$). The general expressions for the respective eigenvectors are:

$$\nu_\pm = \left\{ -\frac{-m + p\alpha \pm \sqrt{\omega}}{2(m + 2p - 1)\alpha}, 1 \right\}.$$

The eigenvalues evaluated at the trivial fixed point, obtained from $\det(J(\mathbf{0}) - \lambda I) = 0$, are $\lambda_\pm^{(a)} = \pm\sqrt{\alpha}$; and the eigenvectors are $\nu_\pm^{(a)} = \{\pm(\sqrt{\alpha})^{-1}, 1\}$. Then, this equilibrium point will be always a saddle because, under the biologically meaningful range (i.e., $0 < \alpha \leq 1$), $\lambda_+^{(a)} > 0$ and $\lambda_-^{(a)} < 0$. As a difference from the model given by Eqs. (3)-(4), the trivial equilibrium is always unstable because no degradation is considered. We note that the fixed points $P_b^* = (0, 1)$ and $P_c^* = (1, 0)$ are the extremes of the equilibria contained in $\mathbf{P}_d^* = (1 - m^*, m^*)$. The eigenvalues of P_b^*, computed from $\det(J(P_b^*) - \lambda I) = 0$, are: $\lambda_1^{(b)} = -1$ and $\lambda_2^{(b)} = 0$, with eigenvectors $\nu_1^{(b)} = \{1, 0\}$ and $\nu_2^{(b)} = \{-1, 1\}$. Moreover, the eigenvalues and the corresponding eigenvectors for the fixed point $P_c^* = (1, 0)$ and the line of equilibria $\mathbf{P}_d^*$, are equal, and given by $\lambda_1^{(c)} = 0$ and $\lambda_2^{(c)} = -\alpha$; and with eigenvectors $\nu_1^{(c)} = \{-1, 1\}$ and $\nu_2^{(b)} = \{0, 1\}$. Note that for the equilibria, $P_{b,c}^*$ and $\mathbf{P}_d^*$ the flows are attracted in one subspace.

The previous results on linear stability analysis are illustrated in Fig. 4. The dependence of the equilibrium concentrations of the (+) and (-) sense strands is shown at increasing values of α. Here, as a difference of the previous model analyzed, such concentrations are dependent on the initial conditions, because of the invariant line of infinite point attractors given by $\mathbf{P}_d^*$ [see the phase portraits displayed in Fig. 4(a)-(d)]. The highest difference between the equilibrium concentration of both strands is found for values of α close to 0, where replication proceeds closer to the stamping machine mode and there is much more production of (+) sense strands. As α grows towards one, approaching to the geometric mode of replication, the two equilibria approach each other. If the initial condition of (+) sense strands is low (as one might expect during viral infection) and $m(0) = 0$, the equilibrium concentrations become very close for the geometric replication. However, if the initial condition for (+) sense strands is increased, the equilibrium concentrations for both strands are not so symmetric as one might expect considering $\alpha \to 1$ (Fig. 4).

IV. CONCLUSIONS

Whether the choice of the mode of replication might confer viruses with increased robustness against the accumulation of deleterious mutations has been a recent subject of debate and some studies have theoretically handled questions related to this hypothesis [16, 17]. Experimental studies giving clues about the model of replication for viruses, mainly obtained from the analysis of mutant distributions, were performed many years ago. For instance, the studies of Luria [21] and Denhardt *et al.* [20], already suggested different models of replication for different viruses. Some other investigations have shown that the replication strategy in viruses as differ-

ent as TuMV [18], Φ6 [22], and ΦX174 [20] is closer to the SMR model. These findings suggest that selection may have favored this replicative scheme operating on independent viral lineages, perhaps as a way of reducing the population mutational load, thus increasing mutational robustness. Together with the mode of replication, several mechanisms have been proposed to contribute to the robustness of RNA virus populations [24]. Robustness, defined as the constancy of the phenotype under mutations or perturbations, has been proposed to arise due to mechanisms like *trans*-complementation or neutrality, intrinsic to virus replication, as well as due to other extrinsic mechanisms consequence of the exploitation of cellular buffering mechanisms like the heat-shock chaperones [25].

In the present study we have analyzed the dynamics of simple models describing the intracellular amplification dynamics of viral RNA taking into account differences in the mode of replication. We first studied a simple model obtained from a dynamical systems successfully used to reproduce experimental data on the accumulation of (+) and (-) sense strands during the amplification phase of TuMV [18]. The conclusions of our previous study were that, for TuMV, the model of replication occurred through a mixed strategy but approximately a 90% of the genomes were produced via SMR. Here we studied the equilibria and stability properties for such a model describing intracellular dynamics of (+) sense ssRNA viruses. We reported a non-degenerate transcritical bifurcation responsible for the extinction of the viral genomes. Such a bifurcation separates two different regimes, given by the coexistence of both types of strands (i.e., condition found in the experimental data) and by the extinction of strands corresponding to an absorbing state. The transition between such phases is governed by a smooth change, suggesting the presence of a second-order phase transition. Other studies have reported this type of transition for quasispecies dynamical systems modeling RNA viruses considering mutation [26, 27]. Moreover, recent investigations have also characterized transcritical bifurcations for quasispecies models considering both mutation and complementation phenomena [28].

A second model only considering the mode of replication was also investigated. This model indicated that when degradation rates of the viral RNAs are not considered, there exists an invariant line of attractors resulting in the coexistence of both strands. Under this dynamics, the equilibrium values of the viral RNAs depend on the initial conditions, as a difference from the first analyzed model, for which the asymptotic dynamics was independent on the initial conditions.

The results reported with the model considering viral RNA degradation reveal that as replication gets closer to the SMR model, the viral strands can suffer the bifurcation and become extinct because of increased degradation rates or decreased replication rate. Although SMR might confer RNA viruses with mutational robustness [16], our study suggests that GR could provide RNA viruses with some other dynamical advantages. For instance, with an increased resistance to the stop of the replication process due to the degradation of the (-) strands in an environment dominated by (+) sense strands, or to the degradation of double-stranded intermediates of replication by the RNA-silencing machinery [29]. In this sense, one might expect that RNA viruses may have evolved towards replication strategies optimizing the interplay between both mutational and dynamical robustness.

This work has been funded by the Human Frontier Science Program Organization grant RGP12/2008, by the Spanish Ministerio de Ciencia e Innovación grants BIO2008-01986 (JAD) and BFU2009-06993 (SFE), and by the Santa Fe Institute. FM is the recipient of a predoctoral fellowship from Universitat Politècnica de València. We also want to thank the hospitality and support of the Kavli Institute for Theoretical Physics (University of California at Santa Barbara), where part of this work was developed (grant NSF PHY05-51164).

[1] Endy, D., Kong, D. & Yin, J. 1997 Intracellular kinetics of a growing virus: a genetically structured simulations for the bacteriophage T7. *Biotechnol. Bioeng.* **55**, 375-389.

[2] You, L., Suthers, P. F. & Yin, J. 2002 Effects of *Escherichia coli* physiology on growth of phage T7 in vivo and in silico. *J. Bacteriol.* **184**, 1888-1894.

[3] Reddy, B. & Yin, J. 1999 Quantitative intracellular kinetics of HIV type 1. *AIDS Res. Hum. Retrovir.* **15**, 273-283.

[4] Dahari, H., Ribeiro, R. M., Rice, C. M. & Perelson, A. S. 2007 Mathematical modeling of subgenomic hepatitis C virus replication in Huh-7 cells. *J. Virol.* **81**, 750-760.

[5] Sidorenko, Y. & Reichl, U. 2004 Structured model of influenza virus replication in MDCK cells. *Biotech. Bioeng.* **88**, 1-14.

[6] Lim, K., Lang, V., Tam, T. & Yin, J. 2006 Model-based design of growth-attenuated viruses. *PLoS Comput. Biol.* **2**, e116.

[7] Krakauer, D. & Komarova, N. 2003 Levels of selection in positive-strand virus dynamics. *J. Evol. Biol.* **16**, 64-73.

[8] Srivastava, R., You, L., Summers, J. & Yin, J. 2002 Stochastic vs. deterministic modeling of intracellular viral kinetics. *J. Theor. Biol.* **218**, 309-321.

[9] Zhdanov, V. P. 2004 Bifurcation in a generic model of intracellular viral kinetics. *J. Phys. A: Math. Gen.* **37**, L63-L66.

[10] Eigen, M., McCaskill, J. & Schuster, P. (1989) The molecular quasispecies. *Adv. Chem. Phys.* **75**, 149-263.

[11] Sanjuán R., Nebot M.R., Chirico N., Mansky L.M. & Belshaw R. 2010 Viral mutation rates. *J. Virol.* **84**, 9733-9748.

[12] Domingo, E., Sabo, D., Taniguchi, T. & Weissmann, C. 1978 Nucleotide sequence heterogeneity of an RNA phage population. *Cell* **13**, 735-44.

[13] Domingo, E., Holland, J. & Ahlquist, P. 1988 RNA genetics (CRC Press, Boca Raton, FL).

[14] Domingo, E. & Holland, J.J. (eds) 1994 Mutation rates and rapid evolution of RNA viruses, in: *The evolutionary biology of RNA viruses* (Ed. Morse, S.) pp. 161-183, Raven Press, New York.

[15] Manrubia, S. C. & Lázaro, E. 2006 Viral evolution. *Phys. of Live Rev.* **3**, 65-91.

[16] Sardanyés, J., Solé, R. V. & Elena, S. F. 2009 Replication mode and landscape topology differentially affect RNA virus mutational load and robustness. *J. Virol.* **83**(23), 12579-89.

[17] Thébaud, G., Chadouef, J., Morelli, M. J., McCauley, J. W. & Haydon, D. T. 2010 The relationship between mutation frequency and replication strategy in positive-sense single-stranded RNA viruses. *Proc. R. Soc. B* **277**, 809-817.

[18] Martínez, F., Sardanyés, J., Elena, S. F. & Daròs, J. A. 2011 Dynamics of a plant RNA virus intracellular accumulation: stamping machine versus geometric replication. *Genetics* **188**, 637-646.

[19] Marro, J. & Dickman, R. 1999 Nonequilibrium phase transitions in Lattice models. Cambridge University Press, Cambridge.

[20] Denhardt, D. & Silver, R. B. 1966 An analysis of the clone size distribution of $\phi X174$ mutants and recombinants. *Virology* **30**, 10-19.

[21] Luria, S. E. 1951 The frequency distribution of spontaneous bacteriophage mutants as evidence for the exponential rate of phage production. *Cold Spring Harbor Symp. Quant. Biol.* **16**, 463-470.

[22] Chao, L., Rang, CU. & Wong, LE. 2002 Distribution of spontaneous mutants and inferences about the replication mode of the RNA bacteriophage Φ6. *J. Virol.* **76**, 3276-3281.

[23] Strogatz, S. H. 2000 *Nonlinear dynamics and chaos.* Westview Press.

[24] Elena, S.F., Carrasco, P., Daròs, J.A. & Sanjuán, R. (2006) Mechanisms of genetic robustness in RNA viruses. *EMBO Rep.* **7**, 168-173.

[25] Jockusch, H., Wiegand, C., Mersch, B. & Rajes, D. 2001 Mutants of Tobacco mosaic virus with temperature-sensitive coat proteins induces heat shock response in tobacco leaves. *Mol. Plant-Microbe Interact.* **14**, 914-917.

[26] Saakian, D. B., Biebricher, C. K. & Hu, C-K. 2009 Phase diagram for the Eigen quasispecies theory with a truncated fitness landscape. *Phys. Rev. E* **79**, 041905.

[27] Tarazona, P. 1992 Error thresholds for molecular quasispecies as phase transitions: from simple landscapes to spin-glass models. *Phys. Rev. A* **45**(8), 60386049.

[28] Sardanyés, J. & Elena, S. F. 2010 Error threshold in RNA quasispecies models with complementation. *J. Theor. Biol.* **265**, 278-286.

[29] Rodrigo, G., Carrera, J., Jaramillo, A. & Elena, S. F. 2011 Optimal viral strategies for bypassing RNA silencing. *J. R. Soc. Interf.* **8**, 257-268.